This is an open access article published under an ACS AuthorChoice License, which permits copying and redistribution of the article or any adaptations for non-commercial purposes.

THE JOURNAL OF PHYSICAL CHEMISTRY C

Article

pubs.acs.org/JPCC

Cocatalyst Effects on Hydrogen Evolution in a Plasmon-Induced Water-Splitting System

Yuqing Zhong, Kosei Ueno, Yuko Mori, Tomoya Oshikiri, and Hiroaki Misawa*

Research Institute for Electronic Science, Hokkaido University, N21, W10, Kita-ku, Sapporo 001-0021, Japan

Supporting Information

ABSTRACT: We explored the performance of hydrogen (H_2) evolution using noble metals or their metal oxides as cocatalysts in the plasmon-induced water-splitting system. Although many studies have employed n-type semiconductor particle systems to investigate cocatalyst effects, evaluating only the catalytic activity of H_2 and oxygen (O_2) evolution has been limited by (1) the difficulty of transferring an electron injected into the conduction band of a semiconductor to a cocatalyst due to the formation of a Schottky barrier when a metallic cocatalyst for H_2 evolution contacts the n-type semiconductor and (2) the potential for a reverse water-splitting reaction, which occurs due to the promotion of the reduction of the evolved O_2 by the cocatalyst. To overcome these limitations, in the present study, we eliminated the adverse effect of the Schottky barrier by obtaining ohmic contact between the semiconductor and the metal or metal oxide cocatalysts, and we used two separate reaction chambers for H_2 and O_2 evolution to avoid reverse water-splitting reactions such as H_2-O_2 recombination or the photoreduction of O_2. A 2−3 nm thick rhodium layer deposited on a platinum board exhibited relatively high performance, a 3-fold increase compared with the absence of a metal or metal oxide cocatalyst thin layer.

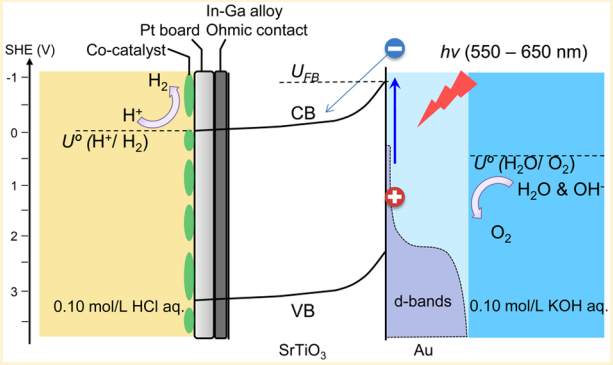

INTRODUCTION

The development of clean, environmentally friendly, and sustainable energy sources as substitutes for fossil fuels has attracted considerable attention. Solar energy will likely play a key role in the development of new energy sources because it is abundant, clean, and uniquely renewable. Hydrogen has attracted significant interest as an energy carrier that offers both high energy capacity and minimal environmental impact. As a sustainable approach for new energy sources, photocatalytic hydrogen production utilizing solar energy is a promising strategy.[1−4]

Photoelectrochemical water splitting has been of great interest since the early 1970s after the first demonstration of water splitting using a titanium dioxide (TiO_2) photoelectrode under ultraviolet radiation by Fujishima and Honda.[5,6] However, a disadvantage of TiO_2 is that it can only be excited by ultraviolet light, i.e., wavelengths shorter than approximately 400 nm, and consequently, only a very small portion of solar radiation (3−5%) can be utilized to drive water splitting. Thus, extension of the absorption wavelength range of TiO_2 to the visible region is critical. Attempts to extend the cutoff wavelength of the water-splitting system to use visible light have included doping,[7−12] defect creation,[13−16] and organic dye or plasmon sensitization.[17−22] We recently demonstrated plasmon-induced water splitting with visible-light irradiation using a strontium titanate ($SrTiO_3$) single-crystal photoelectrode loaded with gold nanoparticles (Au-NPs).[23] We successfully separated the evolution of hydrogen (H_2) and oxygen (O_2) by using two sides of the same $SrTiO_3$ substrate as the cathode and anode.

Investigating cocatalysts for the evolution of H_2 and O_2 is crucial to improve the water-splitting efficiency. Adequate loading of semiconductors with cocatalysts significantly enhances water-splitting activity. However, evaluating the cocatalyst effect for H_2 evolution correctly in water-splitting systems using semiconductor particles is complicated by two factors. First, in H_2 evolution, the Schottky barrier formed by loading metal on the surface of the semiconductor slows the rate of electron transfer from the conduction band of the semiconductor to the metallic cocatalyst due to the increased probability of the back electron-transfer reaction. Such effects are difficult to evaluate because experimental results reflect not only cocatalyst effects but also Schottky barrier effects. Second, reverse water-splitting reactions, such as H_2-O_2 recombination to form H_2O and the photoreduction of O_2, are simultaneously induced in semiconductor particle systems because the cocatalysts also promote the reduction of the evolved O_2. Therefore, evaluating the cocatalyst effect for H_2 evolution may not be simple.

Received: February 20, 2015
Revised: March 20, 2015
Published: April 1, 2015

© 2015 American Chemical Society

DOI: 10.1021/acs.jpcc.5b01720
J. Phys. Chem. C 2015, 119, 8889−8897

To overcome these drawbacks, in the present study, we eliminated the adverse effect of the Schottky barrier by obtaining ohmic contact between the semiconductor and the metal or metal oxide cocatalysts. An In−Ga alloy paste was inserted between the $SrTiO_3$ substrate and the platinum (Pt) board to eliminate the Schottky barrier, and a thin layer of a noble metal or metal oxide cocatalyst for H_2 evolution was subsequently deposited on the surface of the Pt board. H_2 and O_2 were evolved in different chambers with the cathode and anode, respectively. The Au-NP side functioned as the anode for O_2 evolution, whereas the Pt board with the metal or metal oxide cocatalyst side functioned as the cathode for H_2 evolution. Therefore, O_2 and H_2 were separately evolved from the surface and the back of the same $SrTiO_3$ substrate. Eliminating the Schottky barrier effect and preventing the reaction enabled the evaluation of the effects of the cocatalyst on H_2 evolution. In this study, we explored the performance of H_2 evolution using noble metals such as rhodium (Rh) and ruthenium (Ru) or their metal oxides as cocatalysts in the plasmon-induced water-splitting system.

EXPERIMENTAL SECTION

Preparation and Characterization of Au-NPs on the $SrTiO_3$ Substrate. Single-crystal strontium titanate ($SrTiO_3$, 0.05 wt % niobium doped, 10 × 10 × 0.5 mm^3, Furuuchi Chemical Co.) with a (110) surface was used as a semiconductor substrate for water splitting. The $SrTiO_3$ substrate as purchased was rinsed with acetone, methanol, and deionized water in an ultrasonic bath for 5 min, followed by drying under a flow of pure nitrogen. The substrate was subsequently exposed to ozone for 5 min via excimer lamp (PC-01-H, N-Cobo Co.) irradiation under an O_2 atmosphere. A 3 nm thin gold film was deposited on the front side of the $SrTiO_3$ by helicon sputtering (MPS-4000, ULVAC Co.) with a deposition rate of 1 Å/s and annealed at a temperature of 800 °C for 1 h in a nitrogen atmosphere to form Au-NPs on the $SrTiO_3$ surface. The Au-NPs on the $SrTiO_3$ surface were observed by field-emission scanning electron microscopy (FE-SEM, JSM-6700FT, JEOL); the maximum resolution attainable at an electron acceleration voltage of 15 kV was 1 nm. The extinction spectrum of the Au-NPs was monitored using a UV/vis spectrometer (UV-3100, Shimadzu Co.).

Preparation and Characterization of Noble Metal and Metal Oxide Cocatalysts. Pt thin films were sputtered on the back side of the $SrTiO_3$ using a Super Fine Coater ESC-101 (ELIONIX Co.) at a deposition rate of 0.2 Å/s. The Ru and Rh thin films were deposited onto the Pt substrate by a cosputtering system (ACS-4000-C3-HS, ULVAC Co.), and the distance from the target to the substrate was maintained at 150 mm. The targets were ruthenium and rhodium metal with purities of 99.95%. For the Ru and Rh oxide thin-film deposition, a mixture of Ar and O_2 flow was maintained during the sputtering process. However, for the metallic Ru and Rh fabrication, an Ar gas flow rate of 29 sccm was maintained in the absence of O_2 flow. The deposition pressure was maintained at 2.9 × 10^{-1} Pa. The substrate was not heated intentionally during the deposition processes. An X-ray photoemission spectrometer (JPS-9200, JEOL) was used to obtain the X-ray photoemission spectrum (XPS). The center 3 mm × 3 mm area of the substrate surface was used for XPS characterization. The Al Ka line was used as the X-ray source. The C 1s signal was used as an internal reference (284.6 eV). The cross-sectional structure and the elemental distribution of the thin films on the Pt board were analyzed by transmission electron microscopy (TEM) and energy-dispersive X-ray spectroscopy (EDS) on a JEOL JEM-ARM 200F with aberration correction.

Construction of the Water-Splitting Device. An In−Ga alloy (4:1 weight ratio) paste was applied to the back side of the Nb-$SrTiO_3$ substrate to form ohmic contacts. Subsequently, a Pt board (10 × 10 × 0.2 mm^3, 99.98%, Nilaco Co.) with a noble metal or metal oxide thin film on the surface was adhered to the back side of the substrate with Ag paste (D-550, Fujikura Kasei Co.). The water-splitting device contained sealed reaction cells with two solution compartments separated by the Nb-$SrTiO_3$ substrate. The Au-NP-loaded surface was on the front side of the photoelectrode, which was irradiated by visible light to induce O_2 evolution, whereas a Pt board with various cocatalysts was used for H_2 evolution on the back side. To adjust the chemical bias between the H_2- and O_2-evolution chambers, the pH was regulated using hydrochloric acid (HCl) and potassium hydroxide (KOH) aqueous solutions with concentrations of 0.1 mol/dm^3. The volumes of the H_2- and O_2-evolution chambers were 600 and 230 μL, respectively. To maintain the charge balance between the chambers, a salt bridge with 2 wt % agar was used. The pH values of the solutions were examined using a pH meter (AS600, AS ONE Co.).

Quantitative Determination of H_2 and O_2 Evolution. The amounts of evolved O_2 and H_2 were quantitatively determined by gas chromatography−mass spectrometry (GC−MS 2010-plus, Shimadzu Co.) and using a gas chromatograph equipped with a thermal conductivity detector (GC-TCD 2014, Shimadzu Co.), respectively. We analyzed the area counts of the peaks and the identity of the gas based on the calibrated carrier times. The KOH aqueous solution on the O_2 evolution side of the cell was labeled with ^{18}O-water (17.4 atom % isotopic purity) to quantify the oxygen evolution. Ar and N_2 gases were injected into the O_2 evolution side and the H_2 evolution side, respectively, as reference gases for the yield calculations. The GC−MS used to separate and measure O_2 was equipped with an electron ionization (EI) source and a 30.0 m RT-Msieve 5A column (RESTEK); He was used as the carrier gas at a flow rate of 42 mL/min. The gas evolved (5.0 μL) from the front side of the photoelectrode was injected in split mode with a split ratio of 30, and selected ion monitoring (SIM) mode was used for O_2 detection. The column and sample injection temperatures were maintained at room temperature. The EI source temperature was set to 200 °C. The GC-TCD was equipped with a 6.0 m packed column (Shincarbon ST 50/80, Shimadzu Co.), and Ar at a flow rate of 30 mL/min was used as the carrier gas. The gas evolved (10.0 μL) from the back-side chamber was injected. The column and sample injection temperatures were 120 and 200 °C, respectively. The detector temperature was 200 °C. The gold-nanostructured Nb-$SrTiO_3$ substrate was irradiated through an optical window (ϕ6 mm) of the cell by a xenon lamp with a light intensity of 0.32 W/cm^2 and a wavelength from 550 to 650 nm. The incident photon flux was measured using a spectroradiometer (MSR-7000N, Optoresearch Co.).

RESULTS AND DISCUSSION

Water-Splitting Apparatus Construction and Characteristics of the Au-NPs. A 0.05 wt % niobium-doped strontium titanate (Nb-$SrTiO_3$) single crystal with a band gap of 3.2 eV was employed as a semiconductor photoelectrode for

DOI: 10.1021/acs.jpcc.5b01720
J. Phys. Chem. C 2015, 119, 8889−8897

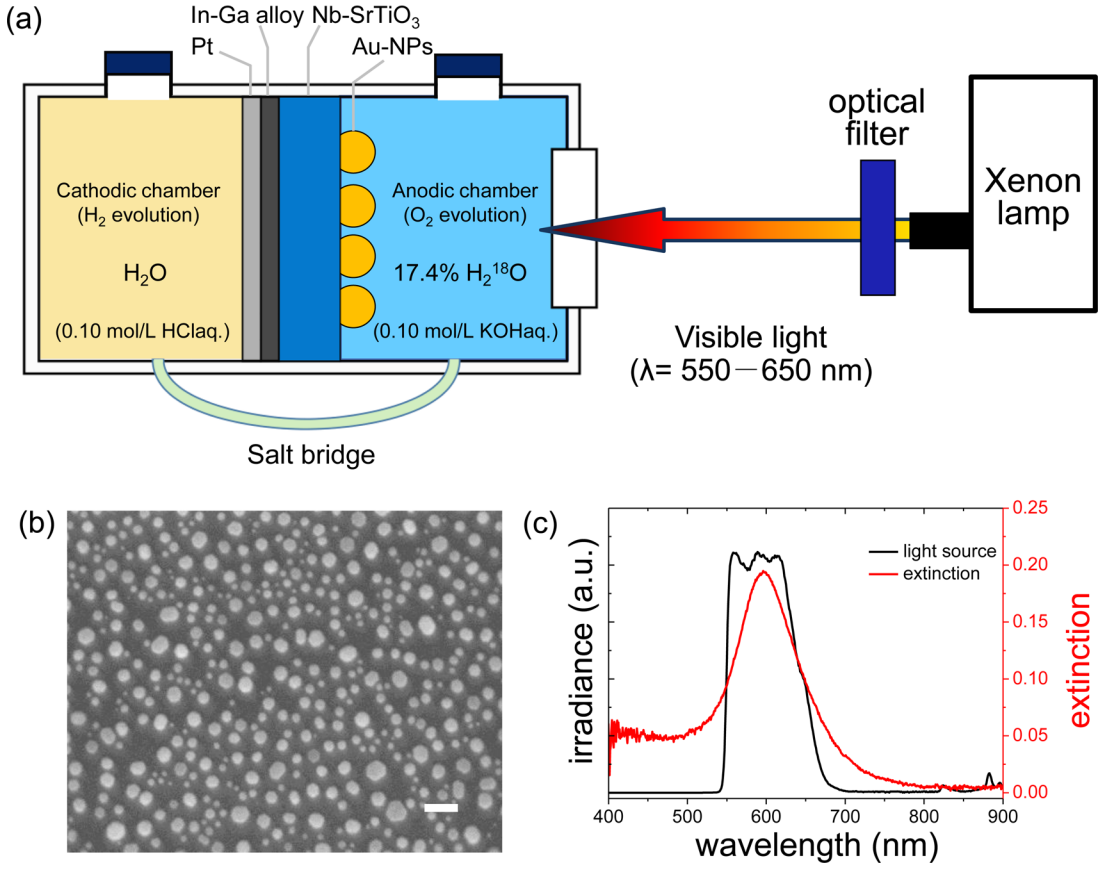

Figure 1. (a) Schematic diagram illustrating the water-splitting device using the Au-NP-loaded Nb-$SrTiO_3$ photoelectrode. (b) The scanning electron microscope top-view image of the Au-NPs on Nb-$SrTiO_3$ prepared using the sputtering and annealing method. The scale bars represent 100 nm. (c) The plasmon resonance band of the Au-NPs loaded on the Nb-$SrTiO_3$ substrate surface and the irradiance wavelength region confined by the sharp-cut filters. The particle size of the Au-NPs was approximately 52 nm, with a standard deviation of approximately 10 nm.

efficient water splitting. A schematic diagram of the water-splitting system using a Au-NP-loaded Nb-$SrTiO_3$ substrate is shown in Figure 1(a). To facilitate the water-splitting reaction, a chemical bias was applied between the two chambers separated by the Nb-$SrTiO_3$ substrate. Specifically, the pH in the front-side chamber (O_2 evolution) was set to 13, while the pH in the back-side chamber (H_2 evolution) was set to 1, using alkaline and acidic aqueous solutions, respectively. According to the Nernst equation, the relationship between the redox potential (U^0) and the pH value at 25 °C is as follows

$$U^0 = U^0\,(\mathrm{pH} = 0) - 0.059 \times \mathrm{pH} \qquad (1)$$

Therefore, the estimated chemical bias applied between the two chambers was 0.71 V.[24,25]

Under irradiation with visible light, plasmon-induced charge separation between Au-NPs and Nb-$SrTiO_3$ and subsequent water oxidation are expected to occur in the front chamber to promote the evolution of O_2. However, in the back-side chamber, H_2 evolution is expected because of the reduction of protons by the electrons injected into the conduction band of Nb-$SrTiO_3$ at the Pt surface used as a cathode material. A conventional salt bridge with 2% agar by weight was employed to maintain the charge balance between these compartments. The pH value did not change before and after irradiation in each experiment, confirming the effectiveness of the salt bridge.

Scanning electron microscope top-view images of the Au-NPs on Nb-$SrTiO_3$ single-crystal substrates are shown in Figure 1(b). The images confirmed that the gold films transformed to discontinuous nanoparticles after annealing at 800 °C in a nitrogen atmosphere, and the interisland spacing was comparable to the nanoparticle size. The diameters of the Au-NPs were distributed nearly symmetrically, with an average size of approximately 52 nm and an estimated standard deviation of 10 nm (Figure S1 in the Supporting Information). Figure 1(c) shows the extinction spectrum of the Au-NPs on the Nb-$SrTiO_3$ substrate and the spectrum of irradiated light whose irradiance wavelength region is defined by sharp-cut optical filters. A localized surface plasmon resonance (LSPR) band peaking at a wavelength of 600 nm was clearly observed. On the basis of this plasmon band peak position, a xenon light spectrally filtered to the wavelengths from 550 to 650 nm with an intensity of 0.32 W/cm^2 was used as a visible-light source in this experiment.

Elimination of the Schottky Barrier Effect between the Semiconductor Material and the H_2 Evolution Cocatalyst. To demonstrate the effect of the Schottky barrier on water-splitting activity in the present system, substrates with different cathode structures with and without In−Ga alloy between $SrTiO_3$ and Pt were fabricated. Their architectures and irradiation time dependences for H_2 and O_2 evolution are shown in Figure 2. For a contrasting structure, a Pt thin film with a thickness of 1 nm was sputtered on the back side of the Nb-$SrTiO_3$ substrate as a substitute for the Pt board. The average thickness of the Pt film was controlled by the sputtering time and determined by an absolute calibration method. The film may have been discontinuous because the film thickness

DOI: 10.1021/acs.jpcc.5b01720
J. Phys. Chem. C 2015, 119, 8889−8897

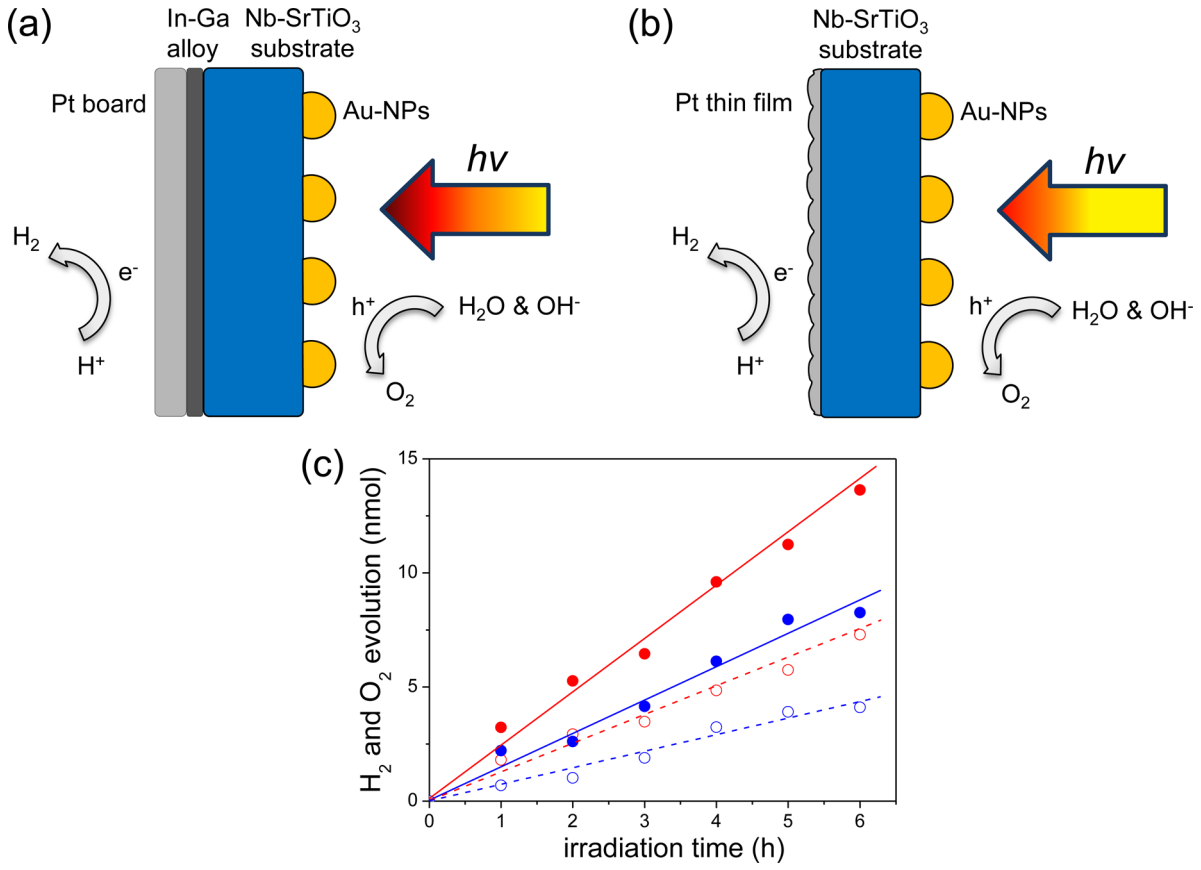

Figure 2. Schematic illustration of the photoelectrode architecture for water splitting using a Pt board (a) and a Pt thin film (b) as the hydrogen evolution site and the dependence of H_2 (solid circles) and O_2 (open circles) evolution on irradiation time (c). The red and blue colors correspond to the Pt board and Pt thin film, respectively.

was set to less than a grain size of 2 nm in this Pt sputtering process.

Under irradiation, the evolution of H_2 and O_2 linearly increased with irradiation time for both structures as shown in Figure 2(c). Stoichiometric evolution of H_2 and O_2 (2:1) was observed in both cases. H_2 and O_2 evolution by the photoelectrode with the Pt thin film was decreased by half compared with the Pt board adhered to Nb-$SrTiO_3$ with an In−Ga alloy. Therefore, it was concluded that the Schottky barrier influenced the water-splitting activity. Without Au-NP decoration, on the other hand, neither H_2 nor O_2 evolved from the Nb-$SrTiO_3$ substrate under the same irradiation conditions. No production of H_2 or O_2 was observed from either photoelectrode architecture for up to 6 h in the absence of irradiation.

Figure 3 depicts the energy band alignment of the composite substrate structure. An excited electron is likely transferred to the conduction band of $SrTiO_3$ immediately following the inter- or intraband transition of the Au-NPs induced by the plasmonically enhanced optical near field. Consequently, a hole is trapped on the surface states of the $SrTiO_3$ near the Au/$SrTiO_3$/water interface; the trapped holes can subsequently induce the oxidation of hydroxyl ions or water molecules efficiently via multielectron transfer.[26−28] A potential gradient was established between the two sides of the Nb-$SrTiO_3$ substrate because a chemical bias was applied by the pH regulation. Under the influence of this potential gradient, the photogenerated electrons injected into the conduction band of $SrTiO_3$ were transferred to the back side and subsequently induced the reduction of protons at the Pt surface. With the Pt nanoparticles on the back side of the Nb-$SrTiO_3$ substrate, there was an undesired Schottky barrier between the Nb-$SrTiO_3$ and Pt, which hindered electron transfer to the cathode, resulting in lower H_2 and O_2 evolution efficiencies. However, when the In−Ga alloy was used to adhere the Pt board to the Nb-$SrTiO_3$ substrate, ohmic contact was very important for H_2 evolution in the plasmon-induced water-splitting system by facilitating electron transfer.

Characteristics of Ru and Rh Thin Films on the Pt Board. A water-splitting system is commonly composed of a semiconductor material and cocatalysts for H_2 and O_2 evolution. The photocatalytic activity of the system is highly dependent on the cocatalysts and their properties, and different cocatalysts must be evaluated.[29−32] The elimination of the Schottky barrier between the cocatalyst and the semiconductor in the composite structure enabled the verification of the performance of various types of cocatalysts.

Ruthenium (Ru)[33−37] and rhodium (Rh)[38−42] species are excellent cocatalysts for H_2 evolution. A thin film of one of these two metals with a thickness of 2−3 nm was deposited by sputtering on the Pt board and served as a cocatalyst for H_2 evolution. By precisely controlling the oxygen flow during the sputtering process, oxides of Ru and Rh were also prepared. A cross-sectional view of a transmission electron microscope (TEM) image confirming the deposition of a Rh thin film with a thickness of 3 nm on the Pt board by sputtering is shown in Figure 4(a), and its corresponding energy-dispersive X-ray spectrometry (EDS) image is shown in Figure 4(b). A cross-sectional view of a TEM image of rhodium oxide with a

DOI: 10.1021/acs.jpcc.5b01720
J. Phys. Chem. C 2015, 119, 8889−8897

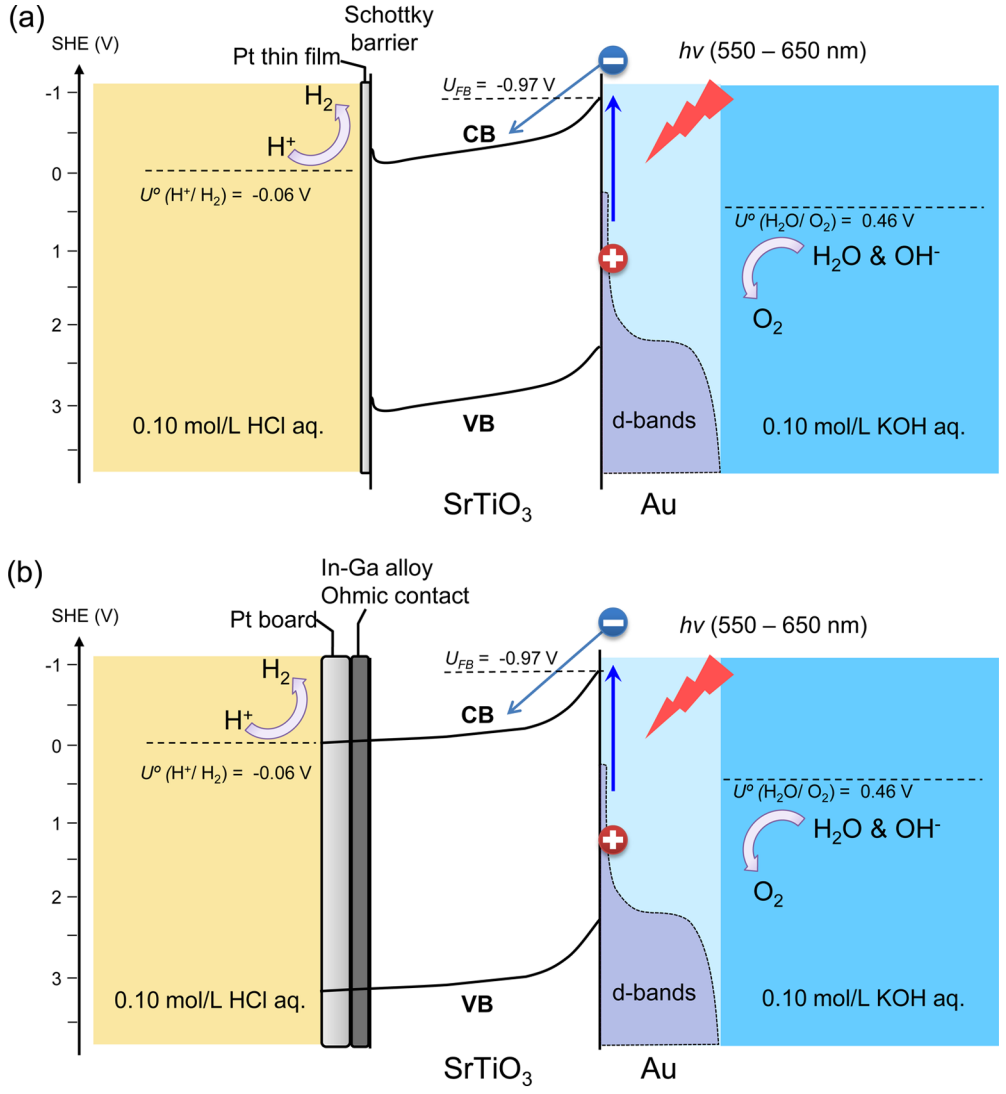

Figure 3. Energy band alignment of the plasmon-induced water-splitting system with the Au-NP-loaded $SrTiO_3$ substrate using Pt nanoparticles (a) and a Pt board (b) as the hydrogen evolution site. U_{FB} and U^0 indicate the flat band potential of $SrTiO_3$ and the redox potentials versus the SHE (standard hydrogen electrode), respectively. The symbols [−] and [+] indicate electrons and holes.

thickness of 4 nm and its corresponding EDS image are shown in Figure 4(c) and (d), respectively. Although a thickness of 4 nm was used instead of 2 or 3 nm films to facilitate TEM observation, importantly, the surface of the rhodium oxide film was clearly rougher than that of the Rh film.

The XPS spectra of the Ru and Rh metals and oxides are shown in Figure 5. Without O_2 flow during the sputtering process, the peak positions of the Ru species were 461.3 and 483.5 eV for Ru $3p_{3/2}$ and $3p_{1/2}$, and the peak positions of the Rh species were 306.5 and 311.3 eV for Rh $3d_{5/2}$ and $3d_{3/2}$, in good agreement with the standard values for the metallic species.[43−45] However, with O_2 flow during the sputtering process, the deposited Ru and Rh species were clearly oxidized, although to a lesser extent than the RuO_2 or Rh_2O_3 bulk references (462.7 and 484.8 eV correspond to the Ru^{4+} oxide RuO_2 and 308.4 and 313.2 eV correspond to the Rh^{3+} oxide Rh_2O_3). Consequently, the oxides will be referred to as RuO_x and RhO_x. XPS measurements confirmed that the ratio of the XPS peak area between Ru 3p and Pt 4f increased almost linearly with increasing RuO_x thickness (Figure S2 in the Supporting Information).

Water-Splitting Performance Using Various Noble Metals and Metal Oxides as the H_2 Evolution Cocatalyst. Water splitting was conducted with all of the cocatalysts and with a bare Pt board as a control experiment. A schematic illustration of the photoelectrode architecture is shown in Figure 6(a). Figure 6(b) depicts the irradiation time dependence of photocatalytic H_2 and O_2 evolution over 2 nm Rh on the Pt board. Stoichiometric evolution of H_2 and O_2 (2:1) was still observed for the Rh cocatalyst. Thus, noble metals deposited on Pt do not undergo any side reactions and work well as cocatalysts for H_2 evolution. Figure 6(b) also shows the result of recycling reactions to verify the stability of the water-splitting system. Significantly, the reaction proceeded with no noticeable deactivation in the 4-round recycling reactions with irradiation time spans up to more than 80 h, demonstrating the good stability of the present architecture. Hence, various noble metals and metal oxides were used as H_2 evolution cocatalysts for comparison, and the corresponding rates of H_2 and O_2 evolution are shown in Figure 6(c). The evolution of both H_2 and O_2 linearly increased with irradiation time in all cases. The quantity of H_2 evolved from the surfaces of all reduction

DOI: 10.1021/acs.jpcc.5b01720
J. Phys. Chem. C 2015, 119, 8889−8897

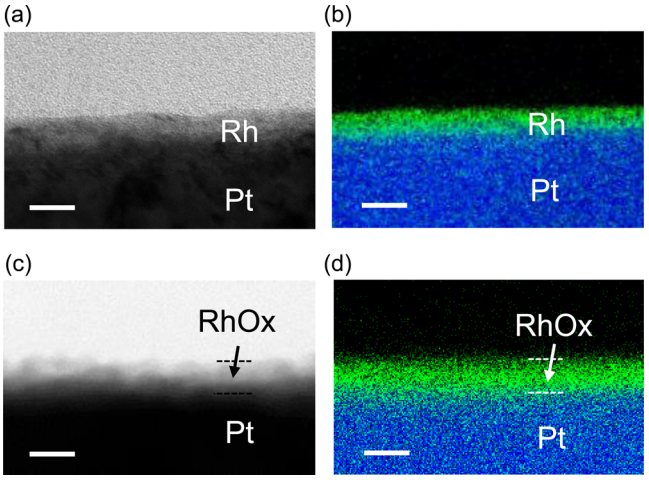

Figure 4. Cross-sectional view of transmission electron microscope images for (a) Rh and (c) RhO_x and the corresponding energy-dispersive X-ray spectrometry (EDS) images for (b) Rh and (d) RhO_x thin films deposited on the Pt board by sputtering. The Rh and Pt signals in the EDS images are indicated by green and blue colors, respectively. The scale bars represent 5 nm in all images.

cocatalysts was twice that of O_2 evolved from the Au nanostructured surface. Therefore, stoichiometric evolution of H_2 and O_2 was clearly demonstrated by various cocatalysts.

Compared with the bare Pt board, the H_2 evolution rate was enhanced by all of the cocatalysts to varying degrees. These cocatalysts are thought to facilitate electron transfer and reactions with the protons in acidic solution environments. The primary role of the noble-metal or metal-oxide thin films on the Pt board is to offer active sites for H_2 evolution.[46−48] Thus, the results obtained here indicate that the Au-NPs/Nb-$SrTiO_3$/In−Ga alloy/Pt/cocatalyst architecture is a promising candidate for photocatalysis. Similar results were obtained using a cocatalyst film with a thickness of 3 nm. The stability of the noble metal and the metal oxide cocatalysts under visible-light irradiation was confirmed by XPS. Each of the Pt boards with cocatalysts was collected and measured after 24 h of light irradiation. The Ru 3p, Ru 3d, Rh 3p, and Rh 3d XPS spectra did not change after the irradiation of any of the cocatalysts (Figure S3 in the Supporting Information). Therefore, the evaluated noble metals or metal oxides were stable on the Pt board under the present experimental conditions.

To further confirm the function of the ohmic contact, as a comparison, a RuO_x thin film with a thickness of 2 nm was deposited as the H_2 evolution cocatalyst directly on the back side of the Nb-$SrTiO_3$ substrate in the absence of the In−Ga alloy and Pt board. As expected, the water-splitting yield declined markedly in the absence of the In−Ga alloy and Pt board (Figure S4 in the Supporting Information).

Some noble metals and metal oxides deposited on a photocatalyst function as cocatalysts for H_2 evolution even in plasmon-induced water splitting. Ideally, the reaction occurring on such cocatalysts should be H_2 evolution. However, undesirable reverse reactions, such as H_2−O_2 recombination to form H_2O and the photoreduction of O_2, occasionally occur on the surface of such cocatalysts and consequently hinder the forward reaction. Maeda et al. reported that photodeposition of a Cr_2O_3 shell permeable to protons and H_2 but not O_2 on noble metals or metal oxides can prevent these reverse reactions.[49−53] Because of its unique two-chamber structure, the water-splitting system presented in this study can also suppress the reverse reactions by separating the evolution of H_2 and O_2. Furthermore, certain metal oxides, such as RuO_2, can function as both reduction and oxidation sites for water during the water-splitting reaction.[54,55] The separation of the H_2 evolution cocatalyst from the O_2 evolution cocatalyst in two different chambers with different solution environments provides a new means of investigating individual cocatalysts by excluding one influence from another.

The relatively higher yield of H_2 evolution obtained using Rh compared with Ru as a cocatalyst is likely attributable to the difference in the free energy of H_2 adsorption, ΔG_H, which has been associated with H_2 evolution activity for a wide variety of metals and alloys.[56] DFT calculations suggest that the absolute value of ΔG_H for Rh is lower than that for Ru, indicating that Rh cocatalysts enhance H_2 evolution compared with Ru catalysts. Besides, it is known that the valence state of Rh also affects the water-splitting activity, and metallic Rh is a superior core material.[51] Consequently, a thin rhodium layer with a thickness of 2 or 3 nm deposited on a platinum board exhibited relatively high performance, as evidenced by a 3-fold increase compared with the absence of a thin metal or metal oxide cocatalyst layer. In summary, we successfully evaluated the cocatalyst effects on H_2 evolution in a plasmon-induced water-splitting system by eliminating the Schottky barrier effect

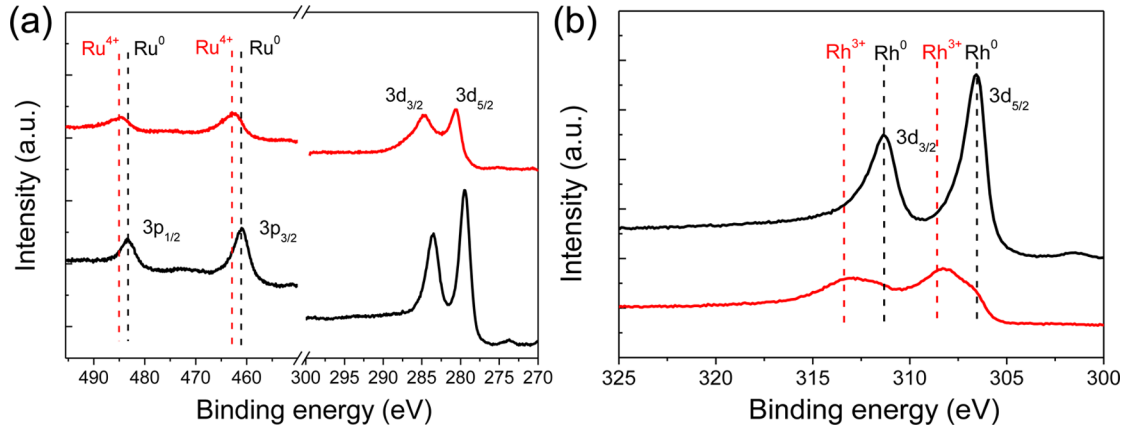

Figure 5. XPS spectra of the (a) Ru 3p and (b) Rh 3d thin films sputtered with (red solid line) and without (black solid line) O_2 flow on the Pt board. The black and red dashed lines indicate the standard metal and oxidation state peak positions of Ru and Rh, respectively.

DOI: 10.1021/acs.jpcc.5b01720
J. Phys. Chem. C 2015, 119, 8889−8897

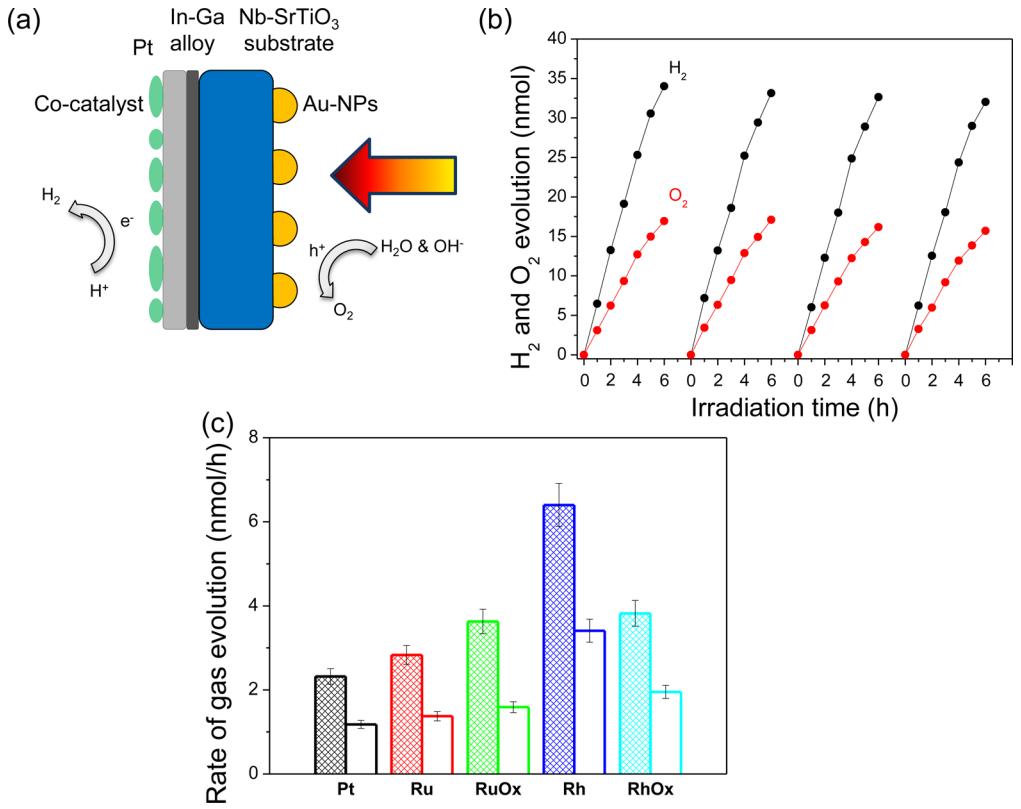

Figure 6. (a) Schematic illustration of the photoelectrode architecture for the overall water splitting using a Pt board decorated with various cocatalysts as the hydrogen evolution site. (b) The recycling irradiation time dependence of H_2 and O_2 evolution in the water-splitting system using Rh deposited on the Pt board with a thickness of 2 nm as the H_2 evolution cocatalyst. (c) Comparison of the rates of H_2 (patterned filled bars) and O_2 evolution (open bars) in the water-splitting system using a Pt board decorated with various cocatalysts.

and separating the two reaction chambers for hydrogen and oxygen evolution to prevent the reverse water-splitting reaction.

CONCLUSIONS

In the present study, we focused on the effect of the cocatalyst on H_2 evolution in plasmon-induced water splitting. Plasmon-induced water splitting with noble metals or metal oxides as cocatalysts for H_2 evolution was achieved in the absence of the Schottky barrier effect or reverse water-splitting reactions. The Schottky barrier between the Pt cathode and the semiconductor material was successfully removed by employing an In−Ga alloy paste. The use of ohmic contact in this system will enable the evaluation of different types of cocatalysts. Deposition of noble metals or metal oxides on the Pt board as H_2 evolution cocatalysts permitted the stoichiometric evolution of H_2 and O_2 in all cases, with varying enhancements of yields. Among the evaluated cocatalysts, metallic Rh had the greatest effect on efficiency, producing a 3-fold improvement compared with the absence of cocatalyst. In addition, the plasmon-induced water-splitting system with a noble metal as a cocatalyst was highly stable for total irradiation times of longer than 80 h. The elucidation and evaluation of the roles of cocatalysts in photocatalytic reactions is critical, and the present study has demonstrated a new method of utilizing various cocatalysts in the design of new and efficient systems for plasmon-induced water splitting.

ASSOCIATED CONTENT

Supporting Information

Statistical analysis of the Au-NP particle size distribution, thickness dependence of partial XPS spectra for RuO_x thin film, stability of various kinds of cocatalysts after water splitting reactions, and comparison of the water-splitting yields with and without In−Ga alloy and Pt board using RuO_x as the H_2 evolution cocatalyst. This material is available free of charge via the Internet at http://pubs.acs.org.

AUTHOR INFORMATION

Corresponding Author

*Tel.: +81-11-706-9358. Fax: +81-11-706-9359. E-mail: misawa@es.hokudai.ac.jp.

Notes

The authors declare no competing financial interest.

ACKNOWLEDGMENTS

This study was supported by funding from the Ministry of Education, Culture, Sports, Science, and Technology of Japan: KAKENHI Grant-in-Aid for Scientific Research (No. 23225006) and the Innovative Areas "Artificial Photosynthesis (AnApple)" (No. 25107501) grant from the Japan Society for the Promotion of Science (JSPS), the Nanotechnology Platform (Hokkaido University), and the Low-Carbon Research Network of Japan.

DOI: 10.1021/acs.jpcc.5b01720
J. Phys. Chem. C 2015, 119, 8889−8897

REFERENCES

(1) Grätzel, M. Artificial Photosynthesis: Water Cleavage into Hydrogen and Oxygen by Visible Light. *Acc. Chem. Res.* **1981**, *14*, 376−384.

(2) Bard, A. J.; Fox, M. A. Artificial Photosynthesis: Solar Splitting of Water to Hydrogen and Oxygen. *Acc. Chem. Res.* **1995**, *28*, 141−145.

(3) Bolton, J. R. Solar Photoproduction of Hydrogen: A Review. *Sol. Energy* **1996**, *57*, 37−50.

(4) Kudo, A. Photocatalysis and Solar Hydrogen Production. *Pure Appl. Chem.* **2007**, *79*, 1917−1927.

(5) Fujishima, A.; Honda, K. Electrochemical Evidence for the Mechanism of the Primary Stage of Photosynthesis. *Bull. Chem. Soc. Jpn.* **1971**, *44*, 1148−1150.

(6) Fujishima, A.; Honda, K. Electrochemical Photolysis of Water at a Semiconductor Electrode. *Nature* **1972**, *238*, 37−38.

(7) Wang, X. H.; Li, J. G.; Kamiyama, H.; Moriyoshi, Y.; Ishigaki, T. Wavelength-Sensitive Photocatalytic Degradation of Methyl Orange in Aqueous Suspension over Iron(III)-doped TiO_2 Nanopowders under UV and Visible Light Irradiation. *J. Phys. Chem. B* **2006**, *110*, 6804−6809.

(8) Sajjad, A. K. L.; Shamaila, S.; Tian, B.; Chen, F.; Zhang, J. Comparative Studies of Operational Parameters of Degradation of Azo Dyes in Visible Light by Highly Efficient WO_x/TiO_2 Photocatalyst. *J. Hazard. Mater.* **2010**, *177*, 781−791.

(9) Asahi, R.; Morikawa, T.; Ohwaki, T.; Aoki, K.; Taga, Y. Visible-light Photocatalysis in Nitrogen-doped Titanium Oxides. *Science* **2001**, *293*, 269−271.

(10) Irie, H.; Watanabe, Y.; Hashimoto, K. Carbon-doped Anatase TiO_2 Powders as a Visible-light Sensitive Photocatalyst. *Chem. Lett.* **2003**, *32*, 772−773.

(11) Li, Q.; Li, Y. W.; Wu, P.; Xie, R.; Shang, J. K. Palladium Oxide Nanoparticles on Nitrogen-Doped Titanium Oxide: Accelerated Photocatalytic Disinfection and Post-Illumination Catalytic "Memory. *Adv. Mater.* **2008**, *20*, 3717−3723.

(12) Chen, X.; Burda, C. The Electronic Origin of the Visible-Light Absorption Properties of C-, N- and S-Doped TiO_2 Nanomaterials. *J. Am. Chem. Soc.* **2008**, *130*, 5018−5019.

(13) Takeuchi, M.; Yamashita, H.; Matsuoka, M.; Anpo, M.; Hirao, T.; Itoh, N.; Iwamoto, N. Photocatalytic Decomposition of NO under Visible Light Irradiation on the Cr-ion-implanted TiO_2 Thin Film Photocatalyst. *Catal. Lett.* **2000**, *67*, 135−137.

(14) Wang, G. M.; Wang, H. Y.; Ling, Y. C.; Tang, Y. C.; Yang, X. Y.; Fitzmorris, R. C.; Wang, C. C.; Zhang, J. Z.; Li, Y. Hydrogen-Treated TiO_2 Nanowire Arrays for Photoelectrochemical Water Splitting. *Nano Lett.* **2011**, *11*, 3026−3033.

(15) Petrik, N. G.; Zhang, Z.; Du, Y.; Dohnálek, Z.; Lyubinetsky, I.; Kimmel, G. A. Chemical Reactivity of Reduced TiO_2(110): The Dominant Role of Surface Defects in Oxygen Chemisorption. *J. Phys. Chem. C* **2009**, *113*, 12407−12411.

(16) Harb, M.; Cavallo, L.; Basset, J.-M. Major Difference in Visible-Light Photocatalytic Features between Perfect and Self-Defective Ta_3N_5 Materials: A Screened Coulomb Hybrid DFT Investigation. *J. Phys. Chem. C* **2014**, *118*, 20784−20790.

(17) O'Regan, B.; Grätzel, M. A Low-cost, High-efficiency Solar Cell Based on Dye-sensitized Colloidal TiO_2 Films. *Nature* **1991**, *353*, 737−740.

(18) Grätzel, M. Dye-sensitized Solar Cells. *J. Photochem. Photobiol. C* **2003**, *4*, 145−153.

(19) Chen, H. M.; Chen, C. K.; Chen, C.-J.; Cheng, L.-C.; Wu, P. C.; Cheng, B. H.; Ho, Y. Z.; Tseng, M. L.; Hsu, Y.-Y.; Chan, T.-S.; et al. Plasmon Inducing Effects for Enhanced Photoelectrochemical Water Splitting: X-ray Absorption Approach to Electronic Structures. *ACS Nano* **2012**, *6*, 7362−7372.

(20) Warren, S. C.; Thimsen, E. Plasmonic Solar Water Splitting. *Energy Environ. Sci.* **2012**, *5*, 5133−5146.

(21) Chen, J.-J.; Wu, J. C. S.; Wu, P. C.; Tsai, D. P. Plasmonic Photocatalyst for H_2 Evolution in Photocatalytic Water Splitting. *J. Phys. Chem. C* **2010**, *115*, 210−216.

(22) Ingram, D. B.; Linic, S. Water Splitting on Composite Plasmonic-Metal/Semiconductor Photoelectrodes: Evidence for Selective Plasmon-Induced Formation of Charge Carriers near the Semiconductor Surface. *J. Am. Chem. Soc.* **2011**, *133*, 5202−5205.

(23) Zhong, Y.; Ueno, K.; Mori, Y.; Shi, X.; Oshikiri, T.; Murakoshi, K.; Inoue, H.; Misawa, H. Plasmon-Assisted Water Splitting Using Two Sides of the Same $SrTiO_3$ Single-Crystal Substrate: Conversion of Visible Light to Chemical Energy. *Angew. Chem., Int. Ed.* **2014**, *53*, 10350−10354.

(24) Zaban, A.; Ferrere, S.; Sprague, J.; Gregg, B. A. pH-Dependent Redox Potential Induced in a Sensitizing Dye by Adsorption onto TiO_2. *J. Phys. Chem. B* **1997**, *101*, 55−57.

(25) Jun, K.; Lee, Y. S.; Buonassisi, T.; Jacobson, J. M. High Photocurrent in Silicon Photoanodes Catalyzed by Iron Oxide Thin Films for Water Oxidation. *Angew. Chem., Int. Ed.* **2012**, *51*, 423−427.

(26) Liu, Z. W.; Hou, W. B.; Pavaskar, P.; Aykol, M.; Cronin, S. B. Plasmon Resonant Enhancement of Photocatalytic Water Splitting Under Visible Illumination. *Nano Lett.* **2011**, *11*, 1111−1116.

(27) Pillai, S.; Catchpole, K. R.; Trupke, T.; Green, M. A. Surface Plasmon Enhanced Silicon Solar Cells. *J. Appl. Phys.* **2007**, *101*, 093105−1−8.

(28) Thomann, I.; Pinaud, B. A.; Chen, Z. B.; Clemens, B. M.; Jaramillo, T. F.; Brongersma, M. L. Plasmon Enhanced Solar-to-Fuel Energy Conversion. *Nano Lett.* **2011**, *11*, 3440−3446.

(29) Maeda, K.; Xiong, A. K.; Yoshinaga, T.; Ikeda, T.; Sakamoto, N.; Hisatomi, T.; Takashima, M.; Lu, D. L.; Kanehara, M.; Setoyama, T.; et al. Photocatalytic Overall Water Splitting Promoted by Two Different Cocatalysts for Hydrogen and Oxygen Evolution under Visible Light. *Angew. Chem., Int. Ed.* **2010**, *49*, 4096−4099.

(30) Iwase, A.; Kato, H.; Kudo, A. Nanosized Au Particles as an Efficient Cocatalyst for Photocatalytic Overall Water Splitting. *Catal. Lett.* **2006**, *108*, 7−10.

(31) Yang, J.; Wang, D.; Han, H.; Li, C. Roles of Cocatalysts in Photocatalysis and Photoelectrocatalysis. *Acc. Chem. Res.* **2013**, *46*, 1900−1909.

(32) Yoshida, M.; Yamakata, A.; Takanabe, K.; Kubota, J.; Osawa, M.; Domen, K. ATR-SEIRAS Investigation of the Fermi Level of Pt Cocatalyst on a GaN Photocatalyst for Hydrogen Evolution under Irradiation. *J. Am. Chem. Soc.* **2009**, *131*, 13218−13219.

(33) Sato, J.; Saito, N.; Nishiyama, H.; Inoue, Y. Photocatalytic Activity for Water Decomposition of Indates with Octahedrally Coordinated d^{10} Configuration. I. Influences of Preparation Conditions on Activity. *J. Phys. Chem. B* **2003**, *107*, 7965−7969.

(34) Sato, J.; Kobayashi, H.; Inoue, Y. Photocatalytic Activity for Water Decomposition of Indates with Octahedrally Coordinated d^{10} Configuration. II. Roles of Geometric and Electronic Structures. *J. Phys. Chem. B* **2003**, *107*, 7970−7975.

(35) Hara, M.; Nunoshige, J.; Takata, T.; Kondo, J. N.; Domen, K. Unusual Enhancement of H_2 Evolution by Ru on TaON Photocatalyst under Visible Light Irradiation. *Chem. Commun.* **2003**, 3000−3001.

(36) Sato, J.; Saito, N.; Yamada, Y.; Maeda, K.; Takata, T.; Kondo, J. N.; Hara, M.; Kobayashi, H.; Domen, K.; Inoue, Y. RuO_2-Loaded β-Ge_3N_4 as a Non-Oxide Photocatalyst for Overall Water Splitting. *J. Am. Chem. Soc.* **2005**, *127*, 4150−4151.

(37) Liu, H.; Yuan, J.; Shangguan, W.; Teraoka, Y. Visible-Light-Responding $BiYWO_6$ Solid Solution for Stoichiometric Photocatalytic Water Splitting. *J. Phys. Chem. C* **2008**, *112*, 8521−8523.

(38) Hata, H.; Kobayashi, Y.; Bojan, V.; Youngblood, W. J.; Mallouk, T. E. Direct Deposition of Trivalent Rhodium Hydroxide Nanoparticles onto a Semiconducting Layered Calcium Niobate for Photocatalytic Hydrogen Evolution. *Nano Lett.* **2008**, *8*, 794−799.

(39) Maeda, K.; Masuda, H.; Domen, K. Effect of Electrolyte Addition on Activity of $(Ga_{1-x}Zn_x)(N_{1-x}O_x)$ Photocatalyst for Overall Water Splitting under Visible Light. *Catal. Today* **2009**, *147*, 173−178.

(40) Maeda, K.; Teramura, K.; Lu, D.; Takata, T.; Saito, N.; Inoue, Y.; Domen, K. Characterization of Rh-Cr Mixed-Oxide Nanoparticles Dispersed on $(Ga_{1-x}Zn_x)(N_{1-x}O_x)$ as a Cocatalyst for Visible-Light-Driven Overall Water Splitting. *J. Phys. Chem. B* **2006**, *110*, 13753−13758.

DOI: 10.1021/acs.jpcc.5b01720
J. Phys. Chem. C 2015, 119, 8889−8897

(41) Maeda, K.; Teramura, K.; Masuda, H.; Takata, T.; Saito, N.; Inoue, Y.; Domen, K. Efficient Overall Water Splitting under Visible-Light Irradiation on $(Ga_{1-x}Zn_x)(N_{1-x}O_x)$ Dispersed with Rh-Cr Mixed-Oxide Nanoparticles: Effect of Reaction Conditions on Photocatalytic Activity. *J. Phys. Chem. B* **2006**, *110*, 13107−13112.
(42) Maeda, K.; Teramura, K.; Saito, N.; Inoue, Y.; Domen, K. Improvement of Photocatalytic Activity of $(Ga_{1-x}Zn_x)(N_{1-x}O_x)$ Solid Solution for Overall Water Splitting by Co-loading Cr and Another Transition Metal. *J. Catal.* **2006**, *243*, 303−308.
(43) Kezilebieke, S.; Ali, M.; Shadeke, B.; Gunnella, R. Magnetic Properties of Ultrathin $Ni_{81}Fe_{19}$ Films with Ta and Ru Capping Layers. *J. Phys.: Condens. Mater.* **2013**, *25*, 476003−1−6.
(44) Kunimori, K.; Hu, Z.; Uchijima, T.; Asakura, K.; Iwasawa, Y.; Soma, M. Rhodium-niobia Interaction in Niobia-promoted Rh/SiO_2 Catalysts: Formation of $RhNbO_4$ on SiO_2. *Catal. Today* **1990**, *8*, 85−97.
(45) Brinen, J. S.; Melera, A. Electron Spectroscopy for Chemical Analysis (ESCA) Studies on Catalysts. Rhodium on Charcoal. *J. Phys. Chem.* **1972**, *76*, 2525−2526.
(46) Maeda, K.; Lu, D.; Domen, K. Direct Water Splitting into Hydrogen and Oxygen under Visible Light by using Modified TaON Photocatalysts with d^0 Electronic Configuration. *Chem.—Eur. J.* **2013**, *19*, 4986−4991.
(47) Jaramillo, T. F.; Jørgensen, K. P.; Bonde, J.; Nielsen, J. H.; Horch, S.; Chorkendorff, I. Identification of Active Edge Sites for Electrochemical H_2 Evolution from MoS_2 Nanocatalysts. *Science* **2007**, *317*, 100−102.
(48) Zong, X.; Yan, H.; Wu, G.; Ma, G.; Wen, F.; Wang, L.; Li, C. Enhancement of Photocatalytic H_2 Evolution on CdS by Loading MoS_2 as Cocatalyst under Visible Light Irradiation. *J. Am. Chem. Soc.* **2008**, *130*, 7176−7177.
(49) Sakamoto, N.; Ohtsuka, H.; Ikeda, T.; Maeda, K.; Lu, D.; Kanehara, M.; Teramura, K.; Teranishi, T.; Domen, K. Highly Dispersed Noble-metal/Chromia (Core/Shell) Nanoparticles as Efficient Hydrogen Evolution Promoters for Photocatalytic Overall Water Splitting under Visible Light. *Nanoscale* **2009**, *1*, 106−109.
(50) Maeda, K.; Teramura, K.; Lu, D.; Saito, N.; Inoue, Y.; Domen, K. Roles of Rh/Cr_2O_3 (Core/Shell) Nanoparticles Photodeposited on Visible-Light-Responsive $(Ga_{1-x}Zn_x)(N_{1-x}O_x)$ Solid Solutions in Photocatalytic Overall Water Splitting. *J. Phys. Chem. C* **2007**, *111*, 7554−7560.
(51) Maeda, K.; Sakamoto, N.; Ikeda, T.; Ohtsuka, H.; Xiong, A.; Lu, D.; Kanehara, M.; Teranishi, T.; Domen, K. Preparation of Core-Shell-Structured Nanoparticles (with a Noble-Metal or Metal Oxide Core and a Chromia Shell) and Their Application in Water Splitting by Means of Visible Light. *Chem.—Eur. J.* **2010**, *16*, 7750−7759.
(52) Maeda, K.; Teramura, K.; Lu, D.; Saito, N.; Inoue, Y.; Domen, K. Noble-Metal/Cr_2O_3 Core/Shell Nanoparticles as a Cocatalyst for Photocatalytic Overall Water Splitting. *Angew. Chem., Int. Ed.* **2006**, *45*, 7806−7809.
(53) Yoshida, M.; Takanabe, K.; Maeda, K.; Ishikawa, A.; Kubota, J.; Sakata, Y.; Ikezawa, Y.; Domen, K. Role and Function of Noble-Metal/Cr-Layer Core/Shell Structure Cocatalysts for Photocatalytic Overall Water Splitting Studied by Model Electrodes. *J. Phys. Chem. C* **2009**, *113*, 10151−10157.
(54) Lee, Y.; Teramura, K.; Hara, M.; Domen, K. Modification of $(Zn_{1+x}Ge)(N_2O_x)$ Solid Solution as a Visible Light Driven Photocatalyst for Overall Water Splitting. *Chem. Mater.* **2007**, *19*, 2120−2127.
(55) Maeda, K.; Abe, R.; Domen, K. Role and Function of Ruthenium Species as Promoters with TaON-Based Photocatalysts for Oxygen Evolution in Two-Step Water Splitting under Visible Light. *J. Phys. Chem. C* **2011**, *115*, 3057−3064.
(56) Greeley, J.; Jaramillo, T. F.; Bonde, J.; Chorkendorff, I.; Norskov, J. K. Computational High-throughput Screening of Electrocatalytic Materials for Hydrogen Evolution. *Nat. Mater.* **2006**, *5*, 909−913.

DOI: 10.1021/acs.jpcc.5b01720
J. Phys. Chem. C 2015, 119, 8889−8897